Deep–Sea Research I 206 (2024) 104247

Contents lists available at ScienceDirect

Deep-Sea Research Part I

journal homepage: www.elsevier.com/locate/dsri

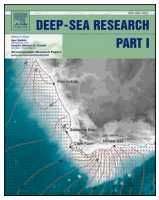

The microbial lipid signature in sediments and chimneys within a back-arc basin hydrothermal system south of the Antarctic Polar Front

Maria T. Hernández-Sánchez [a,b,c,*], Laura Hepburn [d], Michael J. Stock [d], Douglas P. Connelly [d], Richard D. Pancost [a,b,c]

[a] Organic Geochemistry Unit, School of Chemistry, University of Bristol, Cantock's Close, Bristol, BS8 1TS, UK
[b] School of Earth Sciences, University of Bristol, Wills Memorial Building, Bristol, BS8 1RL, UK
[c] The Cabot Institute for the Environment, University of Bristol, Royal Fort House, Bristol, BS8 1UH, UK
[d] National Oceanography Centre, Waterfront Campus, European Way, Southampton, SO14 3ZH, UK

ARTICLE INFO

Keywords:
Lipid biomarkers
Back-arc hydrothermal systems
Microbial ecology
Southern Ocean

ABSTRACT

The impact of hydrothermal systems on surrounding sedimentary microbial communities is not well understood and previous work has been limited to high temperature vent sites at slow or ultraslow spreading oceanic centres. To build on the current understanding of hydrothermal systems, we explore for the first time the organic geochemistry of the only known back-arc basin hydrothermal system outside the Pacific Ocean: the East Scotia Ridge (ESR), which belongs to the South Georgia and South Sandwich Islands Marine Protected Area. Lipid biomarkers contained in sediments and hydrothermal sulphides along two hydrothermal vent fields north and south of the ESR, respectively, revealed the impact of hydrothermal activity, including both high temperature and low temperature diffusive venting, on sedimentary microbial communities. In the vent field north of the ESR, elevated ring indices of glycerol dialkyl glycerol tetraethers (GDGTs) and proportions of monoalkyl glycerol tetraethers (GMGTs), and a high ratio of total fatty acids (FAs; free plus polar lipids) to putative phytoplankton biomarkers in sediments suggest that high-temperature hydrothermalism has a local impact on surrounding sediments through the input of plume dwelling archaea and bacteria. This impact seems to be restricted to the periphery of the vent source, in agreement with the limited dataset available from slow or ultraslow spreading centres. Likewise, elevated FA to phytoplankton biomarker ratios within a diffusive hydrothermal field south of the ESR suggest an additional input of bacterial biomass relative to background sediments. Our results indicate that low temperature diffusive venting might have a higher impact than previously thought, being locally important in supporting the food chain in deep-sea environments. The distribution of tetraether lipids suggests that a higher proportion of thermophilic archaea thrive in the interior of sulphide chimneys, whereas total FA concentrations and distributions suggest that most bacteria inhabit the exterior chimney layers, where temperature is cooler than the innermost layer in contact with the hydrothermal fluid. Furthermore, differences in total FA concentrations suggest that chimney wall thickness is a control on bacterial abundance through the availability of a higher or lower diversity (and volume) of microhabitats. Our results also indicate that bacteria adapt to increasing temperatures by decreasing their degree of unsaturation. By comparison to GDGT data from other settings, it seems that overall ring indices in hydrothermal deposits are governed by growth temperature, although they might also reflect ecological factors. Our results suggest that hydrothermalism shapes microbial communities within chimneys and surrounding sediments following broadly similar patterns regardless of the type of spreading centre they are located at.

1. Introduction

Hydrothermal vents are formed where hot, mineral-rich water resulting from seawater percolating through cracks and fissures in the subsurface and heated and chemically modified through interaction with the host rock, enters into contact again with cold seawater. Deep-sea hydrothermal vents occur along spreading centres and subduction zones (Beaulieu et al., 2013, 2015). In these areas, reduced gases, metals

* Corresponding author
E-mail address: maite1.hernadezsanchez@gmail.com (M.T. Hernández-Sánchez).

https://doi.org/10.1016/j.dsr.2024.104247
Received 16 June 2023; Received in revised form 17 January 2024; Accepted 20 January 2024
Available online 7 February 2024

and other compounds and elements (e.g. nitrogen, sulfur) dissolved in the vent fluids can be used by chemosynthetic microorganisms as an energy source (Linse et al., 2019; Dick, 2019). In deep environments, these microorganisms might be the foundation of food webs (Govenar, 2012) and, therefore, hydrothermal systems are important in supporting deep sea communities (Dubilier et al., 2008; Middleburg, 2011). Since their discovery in the 1970s, several studies have explored these systems and their impact on the deep sea (Comita and Gagosian, 1984; Simoneit et al., 2004; Fuchida et al., 2014; Marsh et al., 2012, 2013; Hawkes et al., 2013; Rogers et al., 2012; James et al., 2014; Zwirglmaier et al., 2015; Husson et al., 2017; Watanabe et al., 2019; Linse et al., 2019). Some of them have focused on understanding microbial diversity by using culture-dependent and independent approaches (Kormas et al., 2006; Flores et al., 2011; Jaeschke et al., 2012; Reeves et al., 2014; Ding et al., 2017). A few studies have applied lipid biomarkers to reconstruct microbial communities in a diversity of habitats within deep sea hydrothermal systems, including chimneys, sediments, vent fluids and benthic fauna (Schouten et al., 2003; Phleger et al., 2005; Blumenberg et al., 2012; Hu et al., 2012; Jaeschke et al., 2012, 2014; Lincoln et al., 2013; Kellermann et al., 2012; Méhay et al., 2013; Lei et al., 2016; Li et al., 2018; Li et al., 2020; Pan et al., 2016; Sollich et al., 2017; Umoh et al., 2020; Bentley et al., 2022). These geochemical approaches have contributed to better understanding of the functioning of these systems. Most of these studies, however, focused on high temperature hydrothermal systems at slow or ultraslow spreading centres areas, and less is known about the organic geochemistry of hydrothermal systems in intermediate and fast spreading areas and that of low temperature hydrothermal vents. Furthermore, the limited number of organic geochemical studies focused in sedimentary microbiology show that hydrothermal activity has an effect on microbial communities in some settings (e.g. Guaymas Basin, Schouten et al., 2003; Bentley et al., 2022; Hellenic Arc, Sollich et al., 2017), whereas this impact appears to be small in other locations (central and Southwest Indian Ridges: Pan et al., 2016; Umoh et al., 2020; Arctic Mid-Ocean Ridge: Jaeschke et al., 2014). Finally, half of those organic geochemical studies focused on archaeal communities and less attention has been given to bacterial communities.

We surveyed lipid biomarker distributions in an intermediate spreading centre within the Scotia Sea (Southern Ocean): the East Scotia Ridge. For the first time, we explore the lipid composition of the only known back-arc basin hydrothermal system outside the Pacific Ocean (Diehl and Bach, 2020; Diehl and Bach, 2021). By looking at lipid biomarkers we evaluate the impact of high-temperature focused venting and low-temperature diffusive venting on sedimentary microbial diversity and biomass, including bacteria. We also provide the first insights into the microbial assemblages inhabiting different parts of a black smoker structure at the ESR. Furthermore, we perform a comparison with archaeal membrane lipid data available in the literature to decipher major controls on archaeal communities in hydrothermal deposits at a wide scale. This research builds on the scarce information available for one of the largest Marine Protected Areas (MPA): the South Georgia and South Sandwich Islands MPA.

2. Methods

2.1. Study site

The ESR is an intermediate rate back-arc spreading centre located between the Scotia Plate and the South Sandwich Plate, in the East Scotia Sea (Southern Ocean; Fig. 1). Spreading started more than 15 Ma ago (Larter et al., 2003) and currently occurs at rates which vary from 65 to 70 mm yr^{-1} (Thomas et al., 2003). The ridge is comprised of nine main segments (E1 to E9; Livermore et al., 1997; Larter et al., 1998) separated by non-transform discontinuities (Livermore, 2003). Plates E2 and E9, located to the north and south of the ESR, respectively (Fig. 1), have been shown to be hydrothermally active (Rogers et al., 2012) and are the focus of this study. In this area the seafloor is bathed by Weddell Sea Deep Water (Naveira-Garabato et al., 2002), although partially mixed with Lower Circumpolar Deep Water at E2. E2 has a rough bathymetry characterized by a series of staircased, terraced features divided by scarps and by a steepsided fissure that runs from north to south (Rogers et al., 2012). E9 is comparatively flat (Hawkes et al., 2013): the ridge axis presents many fissures that run north-northwest–south-southeast through flat sheet lavas (Rogers et al., 2012).

The vent field at the E2 segment is located between 56° 5.2′ S and 56°

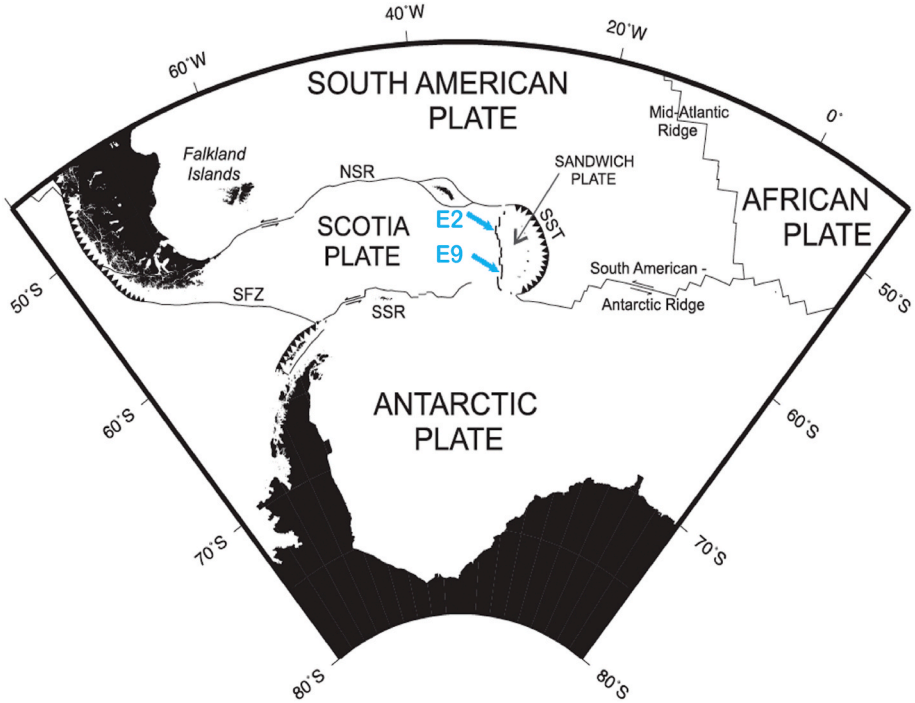

Fig. 1. Location of the ESR, E2 and E9 segments.

5.4′ S and between 30° 19′ W and 30° 19.35′ W at a depth of approximately 2600 m (Rogers et al., 2012). In this area a structure composed of four chimneys up to 10-m high, called "Dog's Head", emits black smoker fluids at temperatures up to 351 °C and a pH ~3.0 (James et al., 2014, Figs. 2A and 3).

The vent field at the E9 segment is located between 60° 02.5′ S and 60° 03.0′ S and between 29° 59.0' W and 29° 58.6 W at a depth of around 2400 m (Rogers et al., 2012). Within this field there are two main areas

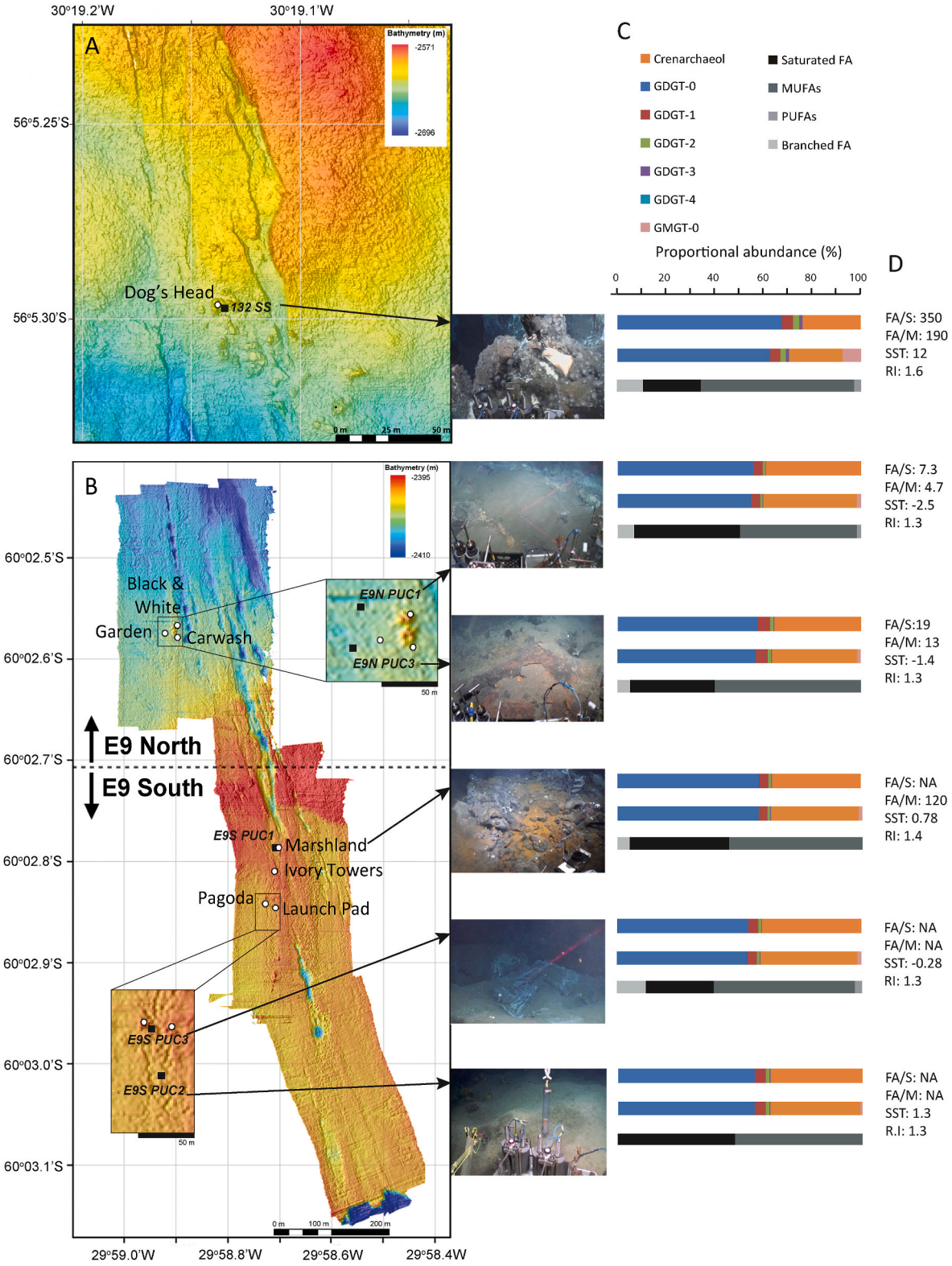

Fig. 2. Hydrothermal vents, and sediment sampling sites in E2 (A) and E9 segments (B). White dots represent venting sites, while black squares represent sediment sampling sites. Panel C shows proportional abundances of GDGTs (first bar), proportional abundances of total identified tetraethers (second bar) and FA proportional abundances (third bar) for each sediment sample. Panel D shows ratios of total FA to total phytoplankton sterols (FA/S), ratios of total FA to total phytoplankton markers (FA/M), TEX_{86}-derived sea surface temperature (SST, in °C) and RIs for each sediment sample analysed. NA means not available.

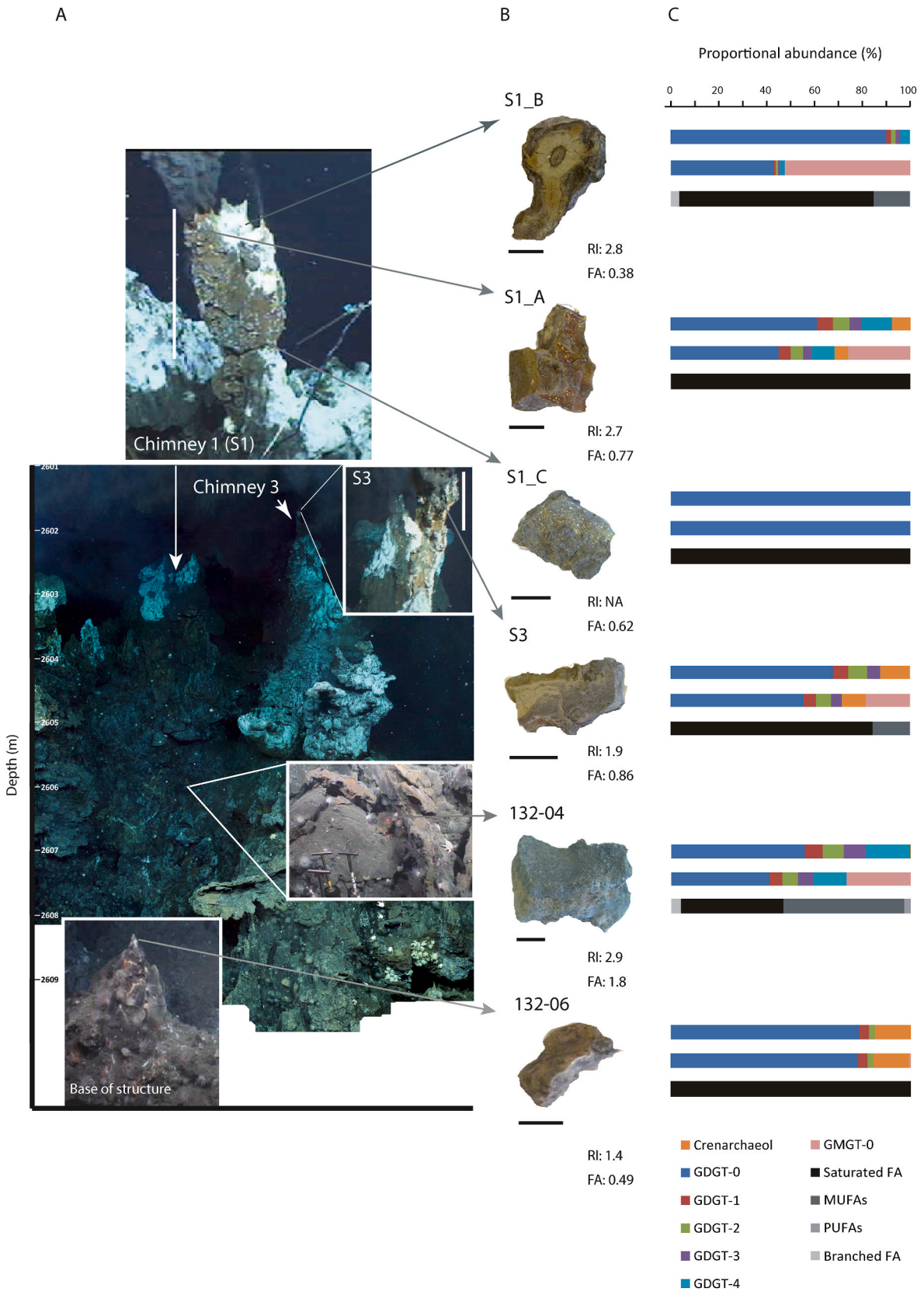

Fig. 3. Panel A shows a photomosaic of the "Dog's Head" structure from Marsh et al. (2013), with sampling locations (ROV video grabs). The white vertical scale lines indicate the length of sections retrieved from chimneys 1 and 3 (S1: 24 cm; S3: 40 cm). Panel B shows images of the samples analysed at each sampling location. The black scale below each image represents 3 cm. Panel C shows proportional abundances of GDGTs (first bar), proportional abundances of total identified tetraethers (second bar) and FA proportional abundances (third bar) for each sulphide sample. FA accounts for the total FA concentration in each sample (in μg g^{-1}) and RI accounts for ring index. NA means not available.

of high temperature hydrothermal activity (Fig. 2B). In the northernmost area of the field (E9 north; E9N hereafter), black smoker fluids of up to 383 °C (and pH ~ 3.5) are emitted from a 10-m multiple vent chimney called "Black and White". In the southern area (E9 south; E9S hereafter), fluids are expelled at high temperature (348-351 °C, and pH: 3.1–3.6; James et al., 2014) at three sites: (i) "Ivory towers", a complex comprised of two black smokers; (b) "Pagoda", a chimney located 50 m south of "Ivory Towers"; and (c) "Launchpad", a site to the east of "Pagoda" where fluids pool beneath a series of flanges (see Fig. 2B). Within the E9 vent field, areas of low temperature (5–20 °C, pH: 5.9–7.6; Marsh et al., 2012; James et al., 2014) diffusive venting occur at "Carwash" and "Garden" (E9N), and at "Marshland" (E9S). The geochemistry of ESR vent fluids is described in detail in Hawkes et al. (2013) and James et al. (2014).

2.2. Sediment and chimney samples

Sediment and chimney samples were collected from E2 and E9 segments on the RRS James Cook (JC42 cruise) during the austral summer of 2010 using the remotely operated vehicle (ROV) *ISIS*. We note that E2 and E9 are bare-rock hydrothermal systems, covered by a thin sediment layer. The thin sediment coverage at the northern segment, E2, allowed the collection of 1 surface sample (132 SS; Fig. 2A) using an ROV-mounted scoop. The sample was retrieved from the base of the high temperature vent structure "Dog's Head", described in section 2.1.

Five sediment samples were recovered from the E9 segment using an ROV-mounted push corer. Samples were collected as close as possible to the vent sites where sediment thickness was sufficient for sampling (Fig. 2B). At E9N, two sediment cores were recovered 47.7 m northwest of the "Black and White" high temperature vent (E9N PUC1) and 24.5 m to the southwest of "Garden" diffusive venting site (E9N PUC3). At E9S, one sediment core was recovered from the "Marshland" (E9S PUC1) low temperature diffusive site and two sediment cores were retrieved 45.5 m southwest of "Launch Pad" (E9S PUC2) and 10.8 m southeast of "Pagoda" (E9S PUC3) high temperature vents (Fig. 2B). Sediment samples were wrapped in aluminium foil, and frozen at −20 °C until analysis. Sediment core tops (top 2 cm) were used for this study.

Chimney material was collected from different parts of the "Dog's Head" black smoker structure only (Fig. 3). The uppermost sections of two active chimneys, chimney 1 (S1) and chimney 3 (S3), were collected using an ROV manipulator arm. Using the same approach, a fragment from a section of an inactive black smoker (132-04) was retrieved from around the half-height of the "Dog's Head" edifice (Fig. 3A), and another (132-06) was collected from the base of the structure. Samples were stored at 4 °C until laboratory analysis.

S1 was further sectioned into three sets of fragments representing: (i) the uppermost part of the main chimney, which is actively venting (sample S1_A); (ii) the end of an extinct, in-filled chimney that branched off chimney 1 (S1_B); and (iii) part of the main chimney 20 cm from the top (S1_C). Samples S1_B and S1_A contain all zones within the chimney wall. Sample S1_C comprises the chimney wall, but the inner layer in contact with the vent fluid represents a small portion of the sample (Fig. 3B).

2.3. Mineralogy

The mineralogy of "Dog's Head" structure has been described previously by James et al. (2014) and here we report additional mineralogical analyses of samples 132-06 and 132-04. Polished blocks and thin sections were made from these samples and analysed using a combination of transmitted and reflected light, with a microscope-mounted optical camera used to image the sample mineralogy. Porosity was visually estimated from reflected light optical observations of polished blocks.

2.4. Biomarker analysis

Lipids were extracted from chimney and sediment samples following a modified Bligh and Dyer (1959) method. Freeze dried samples (~5–8 g for sediments; ~10–18 g for chimneys) were grounded to fine powder and sequentially extracted using a single-phase mixture of MeOH, $CHCl_3$ and aqueous 50 mM phosphate buffer water (2:1:0.8; v/v/v). Phases were separated by adding $CHCl_3$ and buffer water, and the phase containing the lipids was collected. Activated copper turnings were added to the total lipid extract (TLE) and left for 24 h to remove elemental sulfur. The TLE was saponified during 1 h at 70 °C using 0.5M NaOH (95% MeOH) to release bound compounds and further transmethylated with BF_3/MeOH during 30 min at 60 °C to convert free fatty acids into their corresponding methyl esters (FAMEs). The TLE was further silylated with bis (trimethyl) trifluoroacetamide (BSTFA) in pyridine at 70 °C for 1 h to convert alcohols into trimethylsilyl derivatives prior to gas chromatography (GC) and GC-mass spectrometry analysis (GC-MS). GC and GC-MS were performed on the derivatized TLE as described in Hernandez-Sanchez et al. (2010). GC-amenable compounds were quantified using hexadecan-2-ol and *n*-C_{19} standards that had been added to the TLE prior to silylation and GC and GC-MS analyses.

2.5. Tetraether analysis and indices

High performance liquid chromatography-atmospheric pressure chemical ionization-mass spectrometry (HPLC-APCI-MS) for determination of glycerol monoalkyl and dialkyl glycerol tetraethers (GMGTs and GDGTs respectively) was also performed on the TLE, after filtration through a PTFE filter (0.45 μm), and as described in Hernández-Sánchez et al. (2014). Quantification of GDGTs was not performed (because at the time of these analyses, an internal standard was not widely available), but we applied a variety of GDGT based indices to explore changes in environmental conditions and archaeal ecology.

The index of tetraethers consisting of 86 carbon atoms, TEX_{86}, is widely used as a proxy for Sea Surface Temperature (SST) and was calculated for all sediment and chimney samples, as described in Schouten et al. (2002):

$$TEX_{86} = \frac{[\mathrm{GDGT}-2] + [\mathrm{GDGT}-3] + [\mathrm{Cren}']}{[\mathrm{GDGT}-1] + [\mathrm{GDGT}-2] + [\mathrm{GDGT}-3] + [\mathrm{Cren}']} \quad (1)$$

TEX_{86} was translated into SSTs using the formula provided by Schouten et al. (2002):

$$SST = \frac{TEX_{86} - 0.28}{0.015} \quad (2)$$

We have opted not to use more recent calibrations (e.g. Kim et al., 2010), since we only use these indicative values (TEX_{86}-derived SSTs) to distinguish hydrothermal from allochthonous pelagic inputs.

To evaluate tetraether cyclization, the ring index (RI) was calculated as described in Pan et al. (2016):

$$RI = \frac{1\times[GDGT-1] + 2\times[GDGT-2] + 3\times[GDGT-3] + 4\times[GDGT-4]}{[GDGT-1] + [GDGT-2] + [GDGT-3] + [GDGT-4]} \quad (3)$$

3. Results

3.1. Mineralogy

Sample 132-04 is broadly composed of sphalerite (~75%), chalcopyrite (~25%) and pyrite (<1%) ore phases and shows well-developed mineralogical zonation, which appears to reflect different stages of chimney growth (Fig. 1; supplementary information, SI). Different zones can be identified: the side of the sample closest to the inner vent surface is moderately porous (10–20%) and composed of medium-coarse grained chalcopyrite, which radiates into the chimney interior. This

zone (1) grades outwards with coarse chalcopyrite protruding into a second zone (2), dominantly composed of fine-grained sphalerite aggregates with subordinate fine-grained chalcopyrite and minor anhydrite gangue. The next zone (3) is again dominated by sphalerite but with more abundant and coarser, medium-grained chalcopyrite, which occurs as individual crystals. The outer chimney zone (4) comprises fine–medium grained sphalerite aggregates, large quantities of fine-grained chalcopyrite and minor fine-grained pyrite, and contains more abundant anhydrite gangue than inner zones. Throughout the block sphalerite and chalcopyrite are intergrown; where pyrite is present, it is intergrown with both of the other two ore phases (Fig. 1A, SI).

Sample 132-06 is broadly composed of sphalerite (~40%), pyrite (~18%), chalcopyrite (~2%) and covellite (<1%) ore phases with significant barite (~40%). Although minerals are mixed throughout the sample, it has a discontinuous, irregular, banded texture. Sphalerite occurs as fine–coarse grained anhedral masses, intergrown with minor fine grained chalcopyrite and including framboidal pyrite crystals with visible concentric-zoning. Barite has a fibrous texture with thin, elongate grains radiating out from a central point. Covellite is present as individual crystalline aggregates and in places appears to be intergrown with the sphalerite; it often appears to replace the chalcopyrite (Fig. 1B, SI).

3.2. Biomarker concentrations and distributions in sediments

GC-amenable compounds identified in sediments include FAs, sterols (ranging from 26 to 30 carbon atoms), C_{27} and C_{29} 12-hydroxymethyl alkanoates (HA, from now onwards), C_{28} 1,14-diol, hopanoids (17β,21β(H) bishomohopanoic acid (C_{32}) and 17β,21β(H) bishomohopanol (C_{32})), *n*-alkanols and 1-*O*-monoalkyl glycerol ethers (MAGEs). However, not all compounds were detected in all sediments (Table 1; SI).

Total (GC-amenable) biomarker concentrations vary from 0.97 to 48 μg g^{-1} of dry sediment, being highest in sediments collected from E2 and one to two orders of magnitude lower at E9 (Fig. 2A, SI). Within the E9 vent field, the highest concentrations occur in sediments collected from "Marshland" diffusive site (E9N).

The (GC-amenable) lipid distribution is dominated by FAs at all stations, representing 63–98% of the total biomarkers quantified; these represent the pooled abundances of free and bound (including polar lipid) FAs via the saponification of the TLE. Sterols represent 12% to the total biomarker pool at E2 and 14–20% at E9N, while these compounds were not detected (or detected in trace amounts; Table 1, SI) in sediments collected from E9S (Fig. 2B, SI). MAGEs, hopanoids and HA (and diol) represent a small proportion of the total biomarker distribution (varying from 0 to 4.7%; 0.4 to 6.4% and 0 to 5% respectively) and therefore, their distributions are not described in this section. *n*-alkanol proportional abundances are also low (ranging from 0 to 3%), except for one sample collected from E9S, where these compounds represent 28% of the total biomarkers identified.

Fatty acids range in carbon number from 14 to 22 at E2 and from 14 to 28 at E9. Total concentrations are one to two orders of magnitude higher at E2 (47 μg g^{-1}) than at E9 (0.9–8.6 μg g^{-1}). Within the E9 vent field the highest concentrations occur at the "Marshland" diffusive site. The fatty acid distribution is dominated by mono unsaturated fatty acids (MUFAs) at E2, where they represent 63% of the total fatty acid composition, due to the *n*-$C_{16:1}$ and *n*-$C_{18:1}$ components (Fig. 2C). Saturated components are the next most abundant, representing 24% of the total fatty acids. Polyunsaturated fatty acids (PUFAs) represent 3% of the total, and branched fatty acids represent 10%. The E9 sedimentary fatty acid distribution is also dominated by MUFAs, where they range from 48 to 60% of the total fatty acids. Saturated components comprise 28–48% of the total, whereas PUFAs comprise only 0–3% and branched fatty acids comprise 0–12%.

Total sterol concentrations at E2 (1.2 μg g^{-1}) are similar or an order of magnitude higher than at E9N (0.54–1.1 μg g^{-1}), whereas no sterols (or trace amounts: 0.003 μg g^{-1}) were found at E9S (Table 1, SI). C_{27} and C_{29} sterols were identified in sediments recovered from the E2 vent field. A wider range of sterols (C_{26} to C_{30}) were detected in sediments from E9N, although C_{27} and C_{29} components still dominated.

In addition to the GC-amenable compounds, a range of isoprenoidal GDGTs bearing 0 to 3 cyclopentyl moieties (GDGT-0, GDGT-1, GDGT-2 and GDGT-3; Fig. 2C) and crenarchaeol were detected in sediments collected from the E2 and E9 vent fields. GMGTs, in particular GMGT-0, with 0 cyclopentyl moieties, was also detected in all sediment samples. These core lipids represent a mixture of free and some bound compounds after the saponification of the TLE (note that not all GDGTs present as intact polar lipids will have been released by a base hydrolysis). As quantification of tetraethers was not performed, only GDGT/total tetraether distributions and relative abundances are described here. The GDGT distribution is dominated by GDGT-0 in all sediments, representing 68% of the total GDGTs at E2 and 54–58% in sediments recovered at E9 (Table 1 and Fig. 2C). Crenarchaeol is the second most abundant compound, comprising 24% of the total GDGTs in sediments collected at E2, and 35–40% in sediments from E9. Proportions of GDGTs 1–3 in sediments collected from E2 and E9 are much lower, ranging from 5 to 8% of the total GDGTs, and are in general similar to those found in other marine settings (Schouten et al., 2013). Proportional abundances of GDGT-2 and GDGT-3 are highest in sediments collected from E2. GMGT-0 represents 0.80–7.5% of the total tetraethers, with the highest proportional abundance in E2 sediments.

3.3. Biomarker concentrations and distributions in E2 chimney material

Of the GC-amenable lipids, only FAs were detected in all chimney samples. *n*-alkanes and *n*-alkanols were identified in 3 out of the 6 samples, and archaeol in one of the samples (Table 1, SI). Total (GC-amenable) biomarker concentrations are generally much lower (by one to two orders of magnitude) than those found in sediments, varying from 0.49 to 1.7 μg g^{-1} and being highest in the sample collected from the 132-04 chimney (Fig. 2A, SI).

Similar to sediments, the (GC-amenable) lipid distribution is dominated by FAs, representing 73–100% of the total lipids detected. *n*-alkane and *n*-alkanol proportional abundances are lower (less than 9% of the total GC-amenable lipids and often not detected), except for two samples collected from chimney 1, where *n*-alkane and *n*-alkanol proportional abundances constitute 18% (S1_C) and 12% (S1_B) of the total biomarkers quantified, respectively (Fig. 2B, SI). Therefore, their distributions are not described in this section (but detailed in SI). Archaeol accounts for 12% of the total lipids in sample S1_B.

FAs range in carbon number from 15 to 26. Total fatty acid concentrations range from 0.38 to 1.8 μg g^{-1}, and are the highest in sample 132-04. The FA distribution is dominated by saturated components in most samples collected from "Dog's Head" structure (except 132-04), where they represent 81–100% of the total fatty acids. MUFAs were detected in 2 of these samples, and represent around 15% of the total fatty acids, and PUFAs were not detected in any of these samples (Fig. 3). The fatty acid distribution is remarkably different in sample 132-04, dominated by MUFAs, that represent 50% of the total fatty acids through the $C_{16:1}$ and $C_{18:1}$ components. Saturated components represent 43% of the total fatty acids, PUFAs represent 2.7%, and branched fatty acids represent 4.0%.

Isoprenoidal GDGTs bearing 0 to 4 cyclopentyl moieties and crenarchaeol were detected in chimney material. GDGT distributions differ from those found in sediments (Fig. 3) and also vary considerably between samples. GDGT-0 dominates in all samples, comprising 56–100% of the total GDGTs (Table 1; Fig. 3C). In contrast to sediments, crenarchaeol was only detected in samples S3, S1_A, 132-04 and 132-06 where it accounts for 0.14–15% of the total GDGTs. Proportions of GDGTs 1–4 are quite variable among the samples analysed, ranging from 0 to 44% of the total GDGTs. GDGT-4 is present in 3 out of the 6 samples analysed (S1_A, S1_B and 132-04) ranging from 4 to 19% (132-04) of the

Table 1
GDGT proportional abundances, GDGT-derived indices and GDGT-derived SST in ESR sediments and chimneys.

	Proportional abundance							Indices			
Sample ID	GDGT-0	GDGT-1	GDGT-2	GDGT-3	GDGT-4	Cren	Cren'	0/cren	RI	TEX_{86}	TEX_{86}-derived SST (°C)
E2 SS	0.68	0.045	0.024	0.014	0.000	0.24	0.000	2.8	1.6	0.46	12
E9N PUC1	0.56	0.038	0.009	0.002	0.000	0.39	0.000	1.4	1.3	0.24	−2.5
E9N PUC3	0.57	0.050	0.013	0.003	0.000	0.35	0.000	1.6	1.3	0.25	−1.4
E9S PUC1	0.58	0.036	0.011	0.003	0.000	0.36	0.000	1.6	1.4	0.29	0.78
E9S PUC3	0.54	0.040	0.012	0.003	0.000	0.40	0.000	1.3	1.3	0.27	−0.28
E9S PUC2	0.56	0.045	0.015	0.004	0.000	0.38	0.000	1.5	1.3	0.30	1.3
S1_A	0.61	0.066	0.070	0.047	0.13	0.076	0.000	7.9	2.7	0.74	30.3
S1_B	0.90	0.019	0.019	0.020	0.039	0.000	0.000		2.8	0.67	25
S1_C	1.00	0.000	0.000	0.000	0.000	0.000	0.000				
S3	0.68	0.064	0.078	0.054	0.000	0.12	0.000	5.5	1.9	0.79	34
132–06	0.78	0.040	0.024	0.000	0.000	0.15	0.000	5.3	1.4	0.81	35
132–04	0.56	0.075	0.088	0.090	0.19	0.001	0.000	390	2.9	0.71	28

total. GMGT-0 was detected in all chimney samples, except S1_C, and was frequently far more relatively abundant than in sediments, comprising 0.76–52% of the total tetraethers identified. Samples 132-04, S1_A and S1_B have the highest GMGT-0 proportional abundances; in fact, GMGT-0 dominates the total tetraether distribution in S1_B (Fig. 3C).

4. Discussion

4.1. Lipid sources in sediments and influence from hydrothermalism

Sedimentary isoprenoidal GDGTs reflect the input of organic matter sourced from archaea, as these compounds are one of the main constituents of archaeal membranes (together with archaeol; Koga and Morii, 2007). Their distribution ultimately depends on environmental (i.e. temperature and pH) and ecological factors, and several indices have been developed to help describe the relationship between GDGT distributions and environmental conditions (see section 2.5). As GDGTs are ubiquitous in the marine environment, including hydrothermal systems (Schouten et al., 2000, 2013; Hernández-Sánchez et al., 2014; Hu et al., 2012; Pan et al., 2016; Umoh et al., 2020), here we combine these proxies with the ratio of GDGT-0 to crenarchaeol (0/cren from now onwards) to explore the indigeneity and nature of GDGT distributions in sediments. Crenarchaeol is generally considered to be a unique biomarker for widespread pelagic Thaumarchaeota, such that 0/cren ratios are lower than 2 in marine suspended particulate matter and sediments (Schouten et al., 2002, 2013; Hernández-Sánchez et al., 2014; Besseling et al., 2020; Guo et al., 2021). Therefore, elevated values (>2.0) indicate GDGT sources other than Thaumarcheota (e.g. methanogenic Archaea; Blaga et al., 2009).

Likewise, FAs are the main components of living cells in a variety of marine organisms (excluding Archaea), including phytoplankton, bacteria and various faunal groups (Bobbie and White, 1980; Cañavate, 2019). As such, the use of sedimentary FAs (and their distribution) as specific biomarkers is complex. Thus, to determine the most likely sources of FAs and establish a link with hydrothermal activity we explore allochthonous FA inputs. We do so by comparing FA total abundances to lipids that almost certainly derive from phytoplankton: specific sterols (e.g. brassicasterol; Hernandez-Sanchez et al. (2010) and references therein), C_{28} alkyl 1,14-diol and C_{27} and C_{29} 12-hydroxy methyl alkanoates (Sinninghé-Damsté et al., 2003).

4.1.1. Lipid sources in E2 segment sediments

In sediments recovered from E2 the 0/cren ratio is 2.8, higher than values observed for marine Thaumarchaota (0.2–2; Schouten et al., 2002) and the RI (1.6; Table 1) equals the threshold proposed for hydrothermal origin (Pan et al., 2016). Consistent with this, TEX_{86} yields a temperature for overlying surface waters of 12 °C (Table 1), several degrees higher than annual mean SST (1–2 °C; Hogg et al., 2021). This value is also elevated relative to TEX_{86} derived SSTs from western Scotia Sea sediments (Ho et al., 2014), which reproduce overlying SSTs. These results suggest that, in addition to Thaumarchaeotal lipids derived from overlying surface waters, there are other sources of GDGTs. Consistent with this, E2 sediments also contain GMGT-0 in higher proportions than non-hydrothermal sediments (<6%, Schouten et al., 2008), sediments under the influence of low temperature hydrothermalism (1.2% and 1.3%; Jaeschke et al. (2014) and this study at "Marshland", Fig. 2C) and ESR sediments not impacted by hydrothermalism (0.80%–1.6%; see sections 4.1.2 and 4.1.3). The coarse-grained and loosely-packed sediment layer was, at most, a few centimetres thick (Fig. 3A) and exposed to oxic background seawater. Thus, archaea other than methanogens or anaerobes (Schouten et al., 2013; Villanueva et al., 2014) could be producing the excess GDGT-0 and GMGT-0.

Elevated TEX_{86} and RIs could result from archaea growing *in situ* under the influence of advecting high temperature fluids, as recently described around a high temperature hydrothermal complex (Cathedral Hill) in the Guaymas Basin by Bentley et al. (2022). *In situ* growth could also occur due to the mixture of hot hydrothermal fluids with surrounding cold deep water in the periphery of Dogs Head structure, resulting in warmer waters bathing the seafloor in an area of minimal sediment coverage. It was not possible to measure *in situ* temperature at the sampling site (probe failure), but the presence of anemones indicates temperatures below 24 °C (Marsh et al., 2015). Similar temperatures do not seem to impact tetraether distributions (RIs, TEX_{86}, proportional abundance of GMGT-0) in sediments at diffusive vent sites (Jaeschke et al. (2014) and E9S, see next section). Therefore, we propose that although some *in situ* production might take place in E2 sediments, most excess tetraether lipids derive from buoyant plume-dwelling archaea, growing at elevated temperatures (reflected by TEX_{86}, RI and elevated proportional abundances of GMGT-0) reaching the base of "Dog's Head" structure, where sediments were taken from. This hypothesis is in agreement with GDGT distribution in E2 sediments clustering with those of hydrothermal deposits (section 4.2.1; Fig. 4).

Similarly, the ratio of total FA to total phytoplanktonic sterols concentrations (~350; Table 2; Fig. 2A and B) is around 50 times higher than those of marine phytoplankton (Jónasdóttir, 2019). This FA excess could be due to the presence of anemones in E2 sediments (Fig. 2A) partly scooped together with the sediment at the time of sampling. However, this seems unlikely given the absence of anemone parts in E2 sediments, and similar sterol total abundances in E9N sediments, where anemones were absent. Therefore, most FAs appear to derive from other sources, likely bacteria from "Dog's Head" hydrothermal fluids, given our observations for tetraethers.

4.1.2. Lipid sources in E9 segment sediments

In contrast to E2, GDGT distribution in sediments recovered from the E9 segment are consistent with being derived solely from overlying waters. 0/cren ratios and RIs fall within the range observed in typical

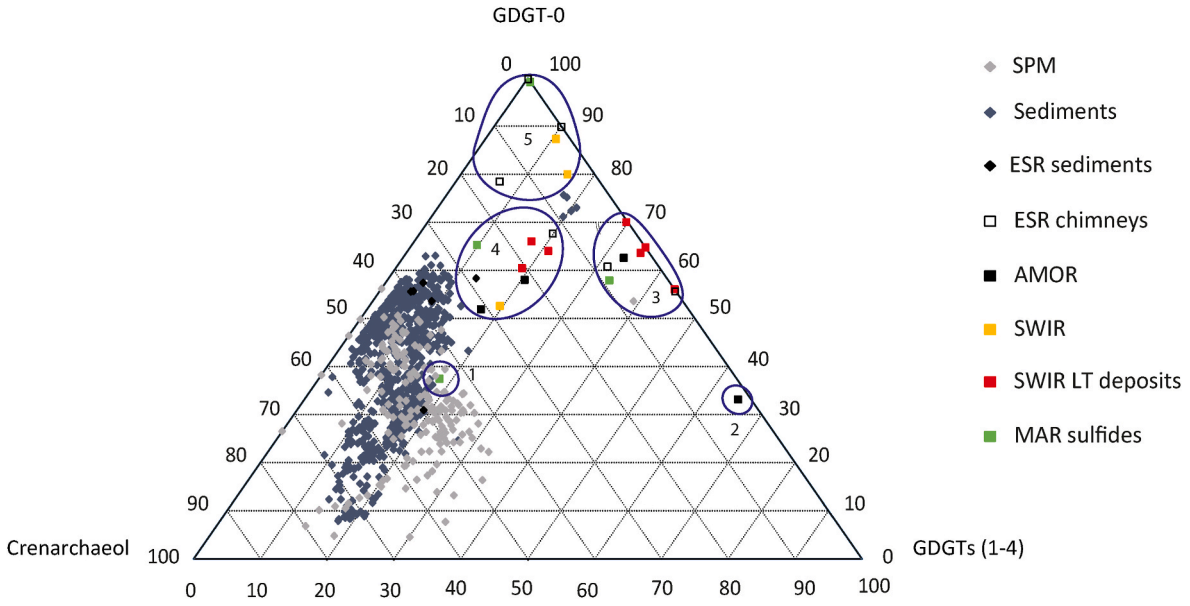

Fig. 4. Ternary diagram showing the distribution of GDGT-0, crenarchaeol and the sum of GDGTs (1–4) in SPM (Turich et al., 2007; Schouten et al., 2012; Hernández-Sánchez et al., 2014; Basse et al., 2014; Kim et al., 2016), sediments (from compilation by Tierney and Tingley (2015) where data was available), and hydrothermal chimneys/deposits in different locations (ESR, Mid Atlantic Ridge (MAR), Arctic Mid Oceanic Ridge (AMOR), Southwest Indian Ridge (SWIR); note that LR refers to low temperature). Numbers refer to each of the groups identified by cluster analysis for hydrothermal samples. SPM and sedimentary data have been plotted for comparison and were not used to define the different groups. Data plotting between groups 3, 4 and 5 represent North Pacific and Bering Sea sediments (Ho et al., 2014), while SPM data plotting within group 3 represent Atlantic Ocean SPM (Basse et al., 2014). In both settings GDGTs have been proposed to derive from methanotrophic or methanogenic archaea.

Table 2
Ratios of total FAs to total phytoplankton sterols and to total phytoplankton markers in sediments.

	Sample ID					
Ratio	E2 SS	E9N PUC1	E9N PUC3	E9S PUC1	E9S PUC3	E9S PUC2
FA/phytoplankton sterols	350	7.3	19			
FA/phytoplankton markers	190	4.7	13	120		

[a]Phytoplankton sterols and phytoplankton markers used to estimate ratios are marked with an asterisk in Table 1 (SI).

marine sediments. Similarly, TEX_{86} derived SSTs range from −2.5 to 1.3 °C (Table 1; Fig. 2A), reproducing (within error; ±2 °C) annual mean SSTs (−1 to 0 °C; Hogg et al., 2021). GMGT-0 proportional abundances also are within values observed in marine sediments (<6%), although we note that those are typically attributed to a benthic source (Schouten et al., 2008).

Total FA concentrations are lower than in E2 sediments and quite variable across the different sites sampled, with ratios of FA/phytoplankton sterols at E9N (7.3 and 19; Table 2) being similar to those of marine phytoplankton (Jónasdóttir, 2019). Phytoplankton specific sterols were detected in trace amounts at one of the southern sites and were absent at the other two; consequently, ratios have not been calculated for E9S sediments. However, ratios of FAs to phytoplankton markers (which includes sterols, HA and diol), exhibit a strikingly similar trend to ratios of FAs to phytoplankton sterols where those were estimated, with the ratio at E2 (ratio of 190) being higher (15–49 times) than values at E9 N (4 and 13); at "Marshland" (E9S) the ratio is 120, similar to that observed at E2. This suggests that at "Marshland" excess FAs are sourced from bacteria growing *in situ* due to the impact of the diffusive vent fluid. Furthermore, total FA concentrations are 7–10 times higher than in the sediments collected from other sites at E9S, located in the proximity of but outside venting points. Thus, at least one E9 site - "Marshland" - contains evidence for elevated bacterial inputs, but not archaeal ones.

4.1.3. *Influence of hydrothermalism in ESR sediments*

Our results suggest that along the ESR, high temperature venting strongly impacts archaeal lipid distributions in E2 but not E9 sediments due to the proximity of E2 sediments to the venting source. Although we have not quantified archaeal biomarkers, the sum of GDGT chromatogram peak areas per gram of sediment, used as a rough approximation of archaeal biomass, is two to three times higher at E2 than at E9 sediments (Table 2, SI). This suggests that high temperature venting enhanced archaeal growth in proximal E2 sediments. High temperature hydrothermalism also enhanced bacterial biomass (based on FA concentrations). Collectively, this suggests an important but highly localised impact from high temperature hydrothermalism on sedimentary microbial communities at the ESR, in agreement with previous (but limited) observations at slow or ultraslow spreading centres. In contrast, low temperature diffusive venting has a more limited impact on E9 sedimentary microbial communities, resulting in increased bacterial biomass grown *in situ* but with no apparent impact on archaeal diversity (TEX_{86} derived SSTs similar to those of overlying waters and 0/cren <2) or biomass (total GDGT chromatogram peak areas per gram of sediment are similar at all E9 sites). We attribute this to the low temperature of the fluid (5–20 °C).

4.2. *Lipids in hydrothermal deposits*

4.2.1. *Global comparison of GDGT distributions*

GDGTs in sulphides show a remarkably different distribution relative to ESR surface sediments (Fig. 3). GMGT proportions are also much higher. In this section we review data available from the literature in order to identify GDGT sources in ESR chimneys and to further decipher the main controls on GDGT distributions in hydrothermal chimneys at a wide scale.

By performing cluster analysis on GDGT proportional abundances (Fig. 3, SI) five different groups were identified (Fig. 4). Group 1 comprises a single sample collected from the Mid Atlantic Ridge (MAR;

CS04); it contains the highest proportional abundance of crenarchaeol, likely resulting from the deposition of planktonic Thaumarchaeota over this chimney after its collapse (Li et al., 2018). Group 2 comprises the interior of an inactive chimney at the Arctic Mid Oceanic Ridge (AMOR; ROV8-2; Jaeschke et al., 2014); it has the lowest and highest proportional abundance of GDGT-0 and GDGTs 1–4, respectively, likely reflecting a strong input of thermophilic Crenarchaeota (Jaeschke et al., 2014).

Group 3 is characterised by elevated proportions of GDGTs 1–4 (30–50%) and includes samples S1_A and 132-04 (ESR) together with deposits collected from the MAR (CS03), the Southwest Indian Ridge (SWIR; SW33, SW37, SW45 and SW46; Pan et al., 2016) and the AMOR (ROV7-1). Li et al. (2018) concluded, based on 16S rRNA analyses, that the dominance of GDGT-0 in a mature MAR chimney (CS03) is due to hyperthermophilic Euryarchaeota, while crenarchaeol derives from thermophilic Thaumarchaeota. Sample S1_A (ESR) has a similar 0/cren ratio suggesting similar communities. Sample 132-04 has much higher 0/cren and 1–4/cren ratios (390 and 305 respectively) than S1_A, indicating even lower contributions of Thaumarchaeota, but they have nearly identical GDGT 1–4 distribution (RIs), which suggests similar GDGT sources. The inclusion of low temperature SWIR deposits in this group likely results from the dominance of non-thermophilic Euryarchaeota (based on 16S rRNA gene analysis; Peng et al., 2011), yielding high 0/cren ratios (but low RIs).

Group 4 includes sample S3 (ESR), together with those collected from the SWIR (TVG1, SW31, SW36, SW41), the AMOR (ROV8-1, ROV7-2), and the MAR (CS02). All of them are characterised by relatively high proportions of crenarchaeol (~10–40%). 0/cren ratios (<2) and similar RIs in samples TVG1 (SWIR) and ROV7-2 (AMOR) indicate GDGTs are likely sourced from pelagic Thaumarchaeota. Elevated 0/cren ratios in the remaining samples suggest additional archaeal groups contributing to the GDGT-0 pool. Sample S3 includes the inner layer of chimney 3 (composed of massive chalchopyrite; James et al., 2014), which suggests that higher abundances of thermophilic communities in the interior of the chimney leads to the excess of GDGT-0 (and elevated 1–4/cren ratios). 16S rRNA analyses indicate that phylotypes associated with Methanosarciniales dominated the archaeal clone libraries in sample SW36 (SWIR; Li et al., 2013) and suggest that besides Thaumarchaeota, Euryarchaeota, mostly Methanosarciniales (mesophiles; Villanueva et al., 2014), are the main GDGT producers in SWIR samples. We note that sediments collected from E2 also plot within this group, consistent with some hydrothermal input of archaea to sediments proposed in section 4.1.1.

Group 5 includes samples S1_B, S1_C and 132-06 (ESR) and samples collected from the SWIR (TVGa, TVGb) and the MAR (CS01), all characterised by their elevated GDGT-0 proportional abundance. Crenarchaeol was not detected in samples CS01, S1_B or S1_C indicating that all GDGTs are being produced by archaeal groups other than Thaumarchaeota. Li et al. (2018) postulated that GDGT-0 dominates in sample CS01 mainly due to (thermophilic) Euyarchaeota (based on 16S rRNA analysis), which could also apply to samples S1_B and S1_C. Sample 132-06 shows a 1–4/cren ratio similar to group 1 but a 0/cren ratio two times higher. This might indicate a similar community (pelagic Thaumarchaeota) producing GDGTs 1–4 and additional sources of GDGT-0 possibly due to higher contributions of archaea that produce GDGT 0.

Crucially, the ESR chimneys and sediments are scattered across three of the five clusters identified in our global analysis. They do not group independently nor do they exhibit any specific features that distinguish them from previous studies. This confirms that ESR archaeal communities – at least as inferred from GDGT distributions – are similar to (or as heterogenous as) those at slow or ultraslow spreading centres.

4.2.2. Tetraether sources in "Dog's Head" structure

The above comparison suggests that the outer part of the wall of "Dog's Head" chimney 1, represented by sample S1_C, is dominated by a community that produces GDGT-0 only (Euryarchaeota) and that (hyper) thermophilic archaea producing GDGTs 0–4 and crenarchaeol likely thrive within the interior of the chimney (S1_A and S1_B). A similar community also inhabits chimney 3. At the base of "Dog's Head" (sample 132-06) most GDGTs seem to derive from pelagic Thaumarchaeota, with excess GDGT-0 derived from other archaea. This is reflected by lower RIs in that sample (132-06) than in samples S1_A, S1_B and 132-04 where RIs are similar, indicating similar vent temperatures at chimneys 1 and 132-04. A lower RI suggests lower archaeal growth temperatures in chimney 3.

GMGT-0 proportional abundance supports the proposed GDGT sources. Although the data set is small, we observe a positive relationship ($r^2 = 0.65$; $p < 0.05$; Fig. 4, SI) with RIs. This suggests that GMGT-0 is produced by (hyper) thermophilic archaea in "Dog's Head" structure, and that their proportional abundances increase with temperature, being highest within the interior part of chimney 1 and lowest or not detected in the outer part of the chimney wall or at the base of the hydrothermal edifice (samples 132-06 and S1_C). Crucially, this suggests that GDGT/GMGT distributions reflect not only the archaeal community structure but also the temperature at which that community is growing – consistent with observations from cultures (Uda et al., 2004; Boyd et al., 2011; Elling et al., 2015) and geothermal systems (Kaur et al., 2011, 2015; Jia et al., 2014).

4.2.3. Controls on GDGT distributions in hydrothermal deposits

4.2.3.1. Temperature. The number of rings in archaeal membrane lipids increases with growth temperature in cultures (Uda et al., 2004; Boyd et al., 2011; Elling et al., 2015). Although this relationship is not unequivocally seen in the field (Pearson et al., 2004), where additional factors (e.g. pH) might also control GDGT distributions (Paraiso et al. (2013) and sections below), it has also been observed in some geothermal springs (Wu et al., 2013; Kaur et al., 2015). This also appears to be true in deep sea hydrothermal systems, where RIs are highest at ESR and AMOR inactive chimneys, and lowest in samples where GDGTs are proposed to be sourced from pelagic Thaumarchaeota. These results suggest temperature as a major driver in shaping archaeal communities in deep hydrothermal deposits.

In general, the highest RIs result from the presence of GDGT-4. In addition to ESR chimneys, up to now GDGT-4 has only been detected in chimneys at the AMOR (Jaeschke et al., 2012, 2014), and in hydrothermal deposits enriched in Fe and/or Si collected from the SWIR (Pan et al., 2016). At the AMOR, barite and silica chimneys as well as black smokers were formed at high temperatures (320–350 °C; Jaeschke et al., 2012, 2014), similar to those of vent fluids discharged at the ESR (323–351 °C; James et al., 2014). In contrast, SWIR deposits analysed by Pan et al. (2016) precipitated at lower temperatures (38.8 and 81.8 °C; Li et al., 2013; Pan et al., 2016). Although these do have lower RIs (1.7–2.46) than those in AMOR (1.95–2.91) and ESR (2.75–2.88) chimneys, it is unclear what drives the production of GDGT-4 in the SWIR. GDGT-4 was not detected in sulphide- and Si- rich SWIR chimneys, which result from higher (300–350 °C) and lower temperature hydrothermal activity, respectively (Li et al., 2018), but was detected in samples that formed at lower temperatures (Pan et al., 2016). Likewise, this compound was not detected in high temperature sulphide chimneys (>300 °C; Li et al., 2018) or lower temperature carbonate chimneys (34–70 °C; Lincoln et al., 2013) at the MAR. These observations suggest that temperature is not the main control on the presence/absence of GDGT-4 in hydrothermal deposits. The absence/presence of GDGDT-4 in certain settings could also result from archaea using membrane lipid architecture strategies, other than increasing the degree of cyclization, to cope with heat stress (e.g. bulking, GMGTs) as observed by Sollich et al. (2017).

4.2.3.2. pH. pH could also control GDGT distribution in thermophilic

archaea, with RIs increasing as pH decreases (Boyd et al., 2011, 2013; Wu et al., 2013; Kaur et al., 2015). At the AMOR, pH is higher (5.5) than at the ESR (3.02–3.05; James et al., 2014) and lower RIs are expected. However, slightly higher RIs are found, indicating that pH is not directly driving the differences in RIs between these settings. There are no pH data available for the SWIR, but it is known that hydrothermal samples precipitated both under high temperature (sulphide chimneys) and lower temperature for the Lei et al. (2016) and Pan et al. (2016) data sets, respectively. Fluids venting from high temperature black smokers at the AMOR and ESR are acidic (Jaeschke et al., 2012; James et al., 2014), whereas diffusive venting allows hydrothermal fluids to mix with seawater leading to lower temperatures and higher pH. Therefore, higher pH is associated with precipitation of low temperature deposits (Pan et al., 2016) relative to sulphides (Lei et al., 2016) at the SWIR. Nonetheless, RIs are lower in the sulphides, suggesting that the pH control on GDGT distributions is also minimal at the SWIR. We acknowledge the limitations of our comparison, noting that the dataset discussed is small, and a range of other factors have not been constrained (e.g. growth rate, redox status; Hurley et al., 2016). As such, we do not conclude that pH exerts no control on GDGT distributions but that this control is subordinate to ecological and temperature factors.

4.2.3.3. Ecological controls on GDGT distributions. Unexpected patterns in RIs and the occurrence/absence of GDGT-4 could reflect different archaeal assemblages rather than growth temperatures or pH, with archaea able to synthesize GDGT-4 growing only in certain settings (or niches within the same setting). Ecological variation arises from intersecting changes in the growth environment and where GDGT-4-producing archaea are able to grow RIs do appear to reflect growth temperature as discussed above; however, GDGT-4 is produced not only by thermophiles but also by mesophyles, at least in low temperature SWIR deposits. Intersecting changes in the growth environment will be profound given the variability in chemistry and redox gradients in deep sea hydrothermal systems (as reflected in the various mineralogies sampled) and could explain higher RIs in low temperature opal deposits relative to sulphide chimneys at the SWIR. However, GDGT-4 has been detected within both sulphide and silica-barite chimneys at the AMOR, and within sulphides collected at the ESR. The conditions of the growth environment could also impact GDGT distributions through their effect on growth rates, with differences in energy conservation strategies leading to lipid remodelling within membranes (Hurley et al., 2016; Sollich et al., 2017). A combination of these factors could explain the presence/absence of GDGT-4 in hydrothermal deposits.

GDGTs with more than 4 rings were not observed at the ESR, although vent temperatures reach values up to 351 °C (James et al., 2014). This is striking as GDGTs with up to 8 rings have been described in hotsprings, despite temperatures being much lower (75 °C; Schouten et al., 2007). This has also been remarked by Jaeschke et al. (2014) for chimneys at the AMOR. Zeng et al. (2019) identified two GDGT synthases (GrsA and GrsB) essential for ring formation and proposed that the number of rings in GDGTs depends on the number of synthase homologues in their genome (e.g. Archaea producing 1–4 rings have one homologue) and on the expression of GrS genes. They further hypothesize that multiple Grs genes that lead to the production of up to 8 rings could be differentially expressed under varying environmental conditions, which supports our observations. An intriguing line of future work will be to ascertain why the presence or expression of Grs genes does not appear widespread in deep sea hydrothermal systems.

4.2.4. GC-amenable compounds in sulphides

The absence of sterols (potentially sourced from plankton and/or fauna) indicates that FAs in sulphides derive from bacteria. FA concentrations are similar in chimneys 1 and 3 indicating similar bacterial biomass. Total FA concentrations are around 100 ng lower in sample S1_C than in S1_A, suggesting that most bacteria thrive in the outer part of the chimney where temperature is lower, as observed in other settings (Hedrick et al., 1992; Schrenk et al., 2003; Edwards et al., 2005; Kormas et al., 2006; Jaeschke et al., 2012; 2014). Total FA concentration is even lower in sample S1_B than in S1_A and S1_C, indicating lower bacterial biomass.

FAs in ESR sulphides have chain lengths ranging from 16 to 25 carbon atoms. Saturated components (mainly $C_{16:0}$ and $C_{18:0}$ alkanoic acids) dominate in chimneys 3 and 1, as observed in other settings (MAR, Simoneit et al., 2004; Blumenberg et al., 2012; AMOR, Jaeschke et al., 2014) and suggesting similar communities. Sample 132-06, at the base of "Dog's Head" has a similar distribution. Within chimney 1, only shorter chain fatty acids (C_{15}, C_{16} and C_{17}) are detected at the vent exit (S1_A), indicating different bacterial assemblages.

Branched (iso and ante iso C_{17}) FAs and MUFAs ($C_{16:1}$ and $C_{18:1}$ alkanoic acids) also occur in samples S3 and S1_B. A higher degree of unsaturation is an adaptation to lower temperatures in bacteria (Siliakus et al. (2017) and references therein), and the presence of these compounds might be an adaptation to lower temperature (lower RI) in chimney 3. This is also a possibility for the extinct chimney represented by sample S1_B, which likely is dominated by a lower temperature "solid community" that uses minerals as energy sources rather than the original "fluid community" that utilized energy from chemicals in the hydrothermal fluids (as demonstrated by Hou et al. (2020)). This could also explain the lower FA concentration in sample S1_B, indicating lower bacterial biomass relative to its active homologues (S1_A and S1_C).

Total FA concentration in sample 132-04 is one order of magnitude higher than in chimneys 1 and 3, indicating much higher bacterial biomass. The dominance of $C_{18:1}$ (32%) alkanoic acid, followed by $C_{16:0}$ (26%) and $C_{16:1}$ (17%) components, also suggests different bacterial assemblages. While chimneys 1 and 3 are composed mainly of chalcopyrite and anhydrite (James et al., 2014), the 134-04 chimney is composed of sphalerite (75%) and chalcopyrite (25%). Additionally, the wall of chimney 132-04 is thicker, and the massive chalcopyrite rich layer coating its inner side represents a much lower proportion of the wall; thus, this sample includes a higher portion of zones beyond this layer, where temperature was lower. Moreover, chimney 132-04 shows a well-developed mineral zonation (see section 3.1) similar to that observed by Schrenk et al. (2003) as well as a similar diversity of FAs.

Schrenk et al. (2003) showed that bacterial biomass was highest in the outer zone of the wall and decreased towards the interior, indicating that most bacterial biomass was located beyond the hot, inner chalcopyrite layer. Our data aligns with that, such that the thick chimney wall of 132-04 results in both cooler and more diverse chimney environments available for bacteria to thrive and associated higher fatty acid concentrations and proportions of unsaturated components. In contrast, the steeper temperature gradient across the thinner wall of chimney 1 yields a lower volume of less diverse habitable microenvironments, which leads to a less diverse microbial community that mainly synthesizes saturated compounds. Moreover, across the entire chimney dataset, bacterial biomass inferred from FAs appears to be lower where archaeal biomass inferred from GDGTs is highest.

5. Conclusions

Hydrothermalism strongly impacts sedimentary microbial communities at the ESR, an intermediate rate spreading centre. High temperature focused venting affects sedimentary microbial diversity and biomass via the input of hydrothermal fluid dwelling archaea and bacteria. The impact of high temperature hydrothermalism in the periphery of the vent source at the ESR is in agreement with previous (but scarce) observations at slow and ultraslow spreading centres: bacterial and especially archaeal growth is stimulated in both sediment-rich and sediment-lean areas around the vent. Intriguingly, low temperature diffusive hydrothermal activity at the ESR also leads to distinct biomarker signatures and concentrations; although such activity does not seem to stimulate archaeal diversity or biomass, it does appear to

have an important impact by stimulating bacterial growth. Thus, although high temperature venting has a greater impact on sedimentary microbial communities, low temperature diffusive venting also affects them through elevated bacterial biomass and could be locally important in supporting the food chain in deep sea environments, having a higher impact than previously thought.

Our analyses of ESR sulphide chimneys complement those from other studies and allow the development of a coherent picture of deep sea hydrothermal system microbial communities and lipids. Although all settings are characterised by heterogeneous microbial communities arising from geochemical and temperature variability, some patterns emerge. A higher proportion of thermophilic archaea (relative to total archaea) appear to thrive in the interior of chimneys, whereas bacterial biomass is constrained to beyond the inner layer of the chimneys in contact with the vent fluid; this is especially true in chimneys with thick walls through the provision of a higher diversity of microhabitats (with different temperatures but also different geochemistry) and volume available to be inhabited. Temperature is a strong (albeit not universal) control on GDGT RIs and the proportions of GMGTs (although the data set is small), and it also appears to be a primary control on bacterial FA unsaturation. A direct control on lipid distributions from pH or mineralogy is less evident, and this almost certainly reflects the complicating role of microbial ecology and growth rates. This similarity between our observations and those in other systems as well as the fact that ESR GDGT distributions are not unique indicates that hydrothermalism shapes chimney microbial communities in broadly similar ways regardless of the nature of the spreading centre.

CRediT authorship contribution statement

Maria T. Hernández-Sánchez: Investigation, Writing – original draft, Writing – review & editing, Conceptualization, Formal analysis, Methodology, Validation. **Laura Hepburn:** Writing – review & editing, Visualization. **Michael J. Stock:** Formal analysis, Writing – review & editing. **Douglas P. Connelly:** Funding acquisition, Writing – review & editing. **Richard D. Pancost:** Funding acquisition, Writing – original draft, Writing – review & editing.

Declaration of competing interest

The authors declare that they have no known competing financial interests or personal relationships that could have appeared to influence the work reported in this paper.

Data availability

Data will be made available on request.

Acknowledgements

We would like to thank the NERC for funding the CheSSo Program (NE/DO1249X/1) and the officers, crew and technical support on RRS James Cook. We are especially grateful to the pilots and technical team of the ROV *ISIS* as well as Dr. Jeff Hawkes for the collection and storage of chimney samples. We would also like to thank Dr. Leigh Marsh for her intellectual contributions and provision of graphical information. Finally, we thank three anonymous reviewers for their suggestions, which led to substantially improve the quality of this manuscript.

Appendix A. Supplementary data

Supplementary data to this article can be found online at https://doi.org/10.1016/j.dsr.2024.104247.

References

Basse, A., Zhu, C., Versteegh, G.J.M., Fischer, G., Hinrichs, K.U., Mollenhauer, G., 2014. Distribution of intact and core tetraether lipids in water column profiles of suspended particulate matter off Cape Blanc, NW Africa. Org. Geochem. 72, 1–13.

Beaulieu, S.E., Baker, E.T., German, C.R., 2015. Where are the undiscovered hydrothermal vents on oceanic spreading ridges? Deep Sea Res. Part II 121, 202–212.

Beaulieu, S.E., Baker, E.T., German, C.R., Maffei, A., 2013. An authoritative global database for active submarine hydrothermal vent fields. Geochem. Geophys. Geosyst. 14 (11), 4892–4905.

Bentley, J.N., Ventura, G.T., Walters, C.C., Sievert, S.M., Seewald, J.S., 2022. The influence of near-surface sediment hydrothermalism on the TEX_{86} tetraether-lipid-based proxy and a new correction for ocean bottom lipid overprinting. Biogeosciences 19, 4459–4477.

Besseling, M.A., Hopmans, E.C., Bale, N.J., Schouten, S., Sinninghe Damsté, J.S., Villanueva, L., 2020. The absence of intact polar lipid-derived GDGTs in marine waters dominated by Marine Group II: implications for lipid biosynthesis in Archaea. Nat. Sci. Rep. 10, 294.

Blaga, C.I., Reichart, G., Heiri, O., Sinninghe Damsté, J., 2009. Tetraether membrane lipid distributions in water-column particulate matter and sediments: a study of 47 European lakes along a north-south transect. J. Palimnol. 41, 523–540.

Bligh, E., Dyer, W., 1959. A rapid method of total lipid extraction and purification. Can. J. Biochem. Physiol. 37, 911–917.

Blumenberg, M., Seifert, R., Buschmann, B., Kiel, S., Thiel, V., 2012. Biomarkers reveal diverse microbial communities in black smoker sulfides from turtle pits (Mid-Atlantic ridge, recent) and Yaman Kasy (Russia, Silurian). Geomicrobiol. J. 29, 66–75.

Bobbie, R.J., White, D.C., 1980. Characterization of benthic microbial community structure by high-resolution gas chromatography of fatty acid methyl esters. Appl. Environ. Microbiol. 39 (6), 1212–1222.

Boyd, E.S., Pearson, A., Pi, Y., Li, W.-J., Zhang, Y., He, L., Zhang, C.L., Geesey, G.G., 2011. Temperature and pH controls on glycerol dibiphytanyl glycerol tetraether lipid composition in the hyperthermophilic crenarchaeon *Acidilobus sulfurireducens*. Extremophiles 15, 59–65.

Boyd, E.S., Hamilton, T.L., Wang, J., He, L., Zhang, C.L., 2013. The role of tetraether lipid composition in the adaptation of thermophilic archaea to acidity. Front. Microbiol. 4, 62.

Cañavate, J.P., 2019. Advancing assessment of marine phytoplankton community structure and nutritional value from fatty acid profiles of cultured microalgae. Rev. Aquacult. 11, 527–549.

Comita, P.B., Gagosian, R.B., 1984. Suspended particulate organic material from hdrothermal vent water at 21 ° N. Nature 304, 450–453.

Dick, G.J., 2019. The microbiomes of deep-sea hydrothermal vents: distributed globally, shaped locally. Nat. Rev. Microbiol. 1, 271–283.

Diehl, A., Bach, W., 2020. MARHYS (marine HYdrothermal solutions). Database: a global compilation of marine hydrothermal vent fluid, end member and seawater compositions. Geochem. Geophys. Geosyst. 21 (12) e2020GC009385.

Diehl, A., Bach, W., 2021. Marhys Database 2.0. https://doi.org/10.1594/PANGAEA.935649. Pangaea.

Ding, J., Zhang, Y., Jiang, H., Leng, H., Xiao, X., 2017. Microbial community structure of deep-sea hydro-thermal vents on the ultraslow spreading Southwest Indian Ridge. Front. Microbiol. 8, 1012.

Dubilier, M., Berin, C., Lott, C., 2008. Symbiotic diversity in marine animals: the art of harnessing chemosynthesis. Nat. Rev. Microbiol. 6, 725–740.

Edwards, K., Bach, W., McCollom, T.M., 2005. Geomicrobiology in oceanography: microbe-mineral interactions at and below the seafloor. Trends Microbiol. 13 (9), 449–456.

Elling, F.J., Könneke, M., Mußmann, M., Greve, A., Hinrichs, K.-U., 2015. Influence of temperature, pH, and salinity on membrane lipid composition and TEX_{86} of marine planktonic thaumarchaeal isolates. Geochim. Cosmochim. Acta 171, 238–255.

Flores, G.E., Campbell, J.H., Kirshtein, J.D., Meneghin, J., Podar, M., Steinberg, J.I., Seewald, J.S., Tivey, M.K., Voytek, M.A., Yang, Z.K., Reysenbach, A., 2011. Microbial community structure of hydrothermal deposits from geochemically different vent fields along the Mid-Atlantic Ridge. Environ. Microbiol. 13, 2158–2171.

Fuchida, S., Mizuno, Y., Masuda, H., Toki, T., Mikita, H., 2014. Concentrations and distributions of amino acids in black and white smoker fluids at temperaturesover 200 °C. Org. Geochem. 66, 98–106.

Govenar, B., 2012. Energy transfer through food webs at hydrothermal vents: linking the lithosphere to the biosphere. Oceanography 25, 246–255.

Guo, J., Yuan, H., Song, J., Qu, B., Xing, J., Wang, Q., Li, X., Duan, L., Li, N., Wang, Y., 2021. Variation of isoprenoid GDGTs in the stratified marine water column: implications for GDGT-based TEX_{86} paleothermometry. Front. Mar. Sci. 8, 715708.

Hawkes, J.A., Connelly, D.P., Gledhill, M., Achterberg, E.P., 2013. The stabilisation and transportation of dissolved iron from high temperature hydrothermal vent systems. Earth Planet. Sci. Lett. 375, 280–290.

Hedrick, D.B., Pledger, R.D., White, D.C., Baross, J.A., 1992. In-situ microbial ecology of hydrothermal vent sediments. FEMS Microbiol. Lett. 101, 1–10.

Hernandez-Sanchez, M.T., Venables, H., Mills, R.A., Wolff, G., Fisher, E.H., Holtvoeth, J., Leng, M.J., Pancost, R.D., 2010. Productivity variations around the Crozet Plateau: a naturally Fe fertilised area of the Southern Ocean. Org. Geochem. 41, 767–778.

Hernández-Sánchez, M.T., Woodward, E.M.S., Taylor, K.W.R., Henderson, G.M., Pancost, R.D., 2014. Variations in GDGT distributions through the water column in the south east Atlantic Ocean. Geochim. Cosmochim. Acta 132, 337–348.

Ho, S.L., Mollenhauer, G., Feitz, S., Martinez-Garcia, A., Lamy, F., Rueda, G., Schipper, K., Méheust, M., Rosell-Melé, A., Stein, R., Tiedemann, R., 2014. Appraisal of TEX_{86} and TEX_{86}^{L} thermometries in subpolar and polar regions. Geochim. Cosmochim. Acta 131, 213–226.
Hou, J., Sievert, S.M., Wang, Y., Seewald, J.S., Natarajan, V.P., Wang, F., Xiao, X., 2020. Microbial succession during the transition from active to inactive stages of deep-sea hydrothermal vent sulfide chimneys. Microbiome 8, 102.
Hogg, O., Downie, A.L., Vieira, R.P., Darby, 2021. Macrobenthic assessment of the South Sandwich Islands reveals a biogeographically distinct polar archipelago. Front. Mar. Sci. 8, 650241.
Hu, J., Meyers, P.A., Chen, G., Peng, P., Yang, Q., 2012. Archaeal and bacterial glycerol dialkyl glycerol tetraethers in sediments from the eastern lau spreading center, south Pacific Ocean. Org. Geochem. 43, 162–167.
Hurley, S.J., Elling, F.J., Könneke, M., Buchwald, C., Wankel, S.D., Santoro, A.E., Lipp, J. S., Hinrich, K.U., Pearson, A., 2016. Influence of ammonia oxidation rate on thaumarchaeal lipid composition and the TEX_{86} temperature proxy. Proc. Natl. Acad. Sci. 13 (28), 7762–7767.
Husson, B., Sarradin, P.M., Zeppilli, D., Sarrazin, J., 2017. Picturing thermal niches and biomass of hydrothermal vent species. Deep Sea Res. Part II 137, 6–25.
Jaeschke, A., Eickmann, B., Lang, S.Q., Bernasconi, S.M., Strauss, H., Früh-Green, G.L., 2014. Biosignatures in chimney structures and sediment from the Loki's Castle low-temperature hydrothermal vent field at the Arctic Mid-Ocean Ridge. Extremophiles 18, 545–560.
Jaeschke, A., Jørgensen, S.L., Bernasconi, S.M., Pedersen, R.B., Thorseth, I.H., Früh-Green, G.L., 2012. Microbial diversity of Loki's Castle black smokers at the Arctic Mid-Ocean Ridge. Geobiology 10, 548–561.
James, R.H., Green, D.R., Stock, M.J., Alker, B.J., Banerjee, N.R., Cole, C., German, C.R., Huvenne, V.A., Powell, A.M., Connelly, D.P., 2014. Composition of hydrothermal fluids and mineralogy of associated chimney material on the East Scotia Ridge back-arc spreading centre. Geochim. Cosmochim. Acta 139, 47–71.
Jia, C., Zhang, C.L., Xie, W., Wang, J., Li, F., Wang, S., Dong, H., Li, W., Boyd, E., 2014. Differential temperature and pH controls on the abundance and composition of H-GDGTs in terrestrial hot springs. Org. Geochem. 75, 109–121.
Jónasdóttir, S.H., 2019. Fatty acid profiles and production in marine phytoplankton. Mar. Drugs 17 (3), 151.
Kaur, G., Mountain, B.W., Hopmans, E.C., Pancost, R.D., 2011. Preservation of microbial lipids in Geothermal sinters. Astrobiology 11, 3.
Kaur, G., Mountain, B.W., Stott, M.B., Hopmans, E.C., Pancost, R.D., 2015. Temperature and pH control on lipid composition of silica sinters from diverse hot springs in the Taupo Volcanic Zone, New Zealand. Extremophiles 19, 327–344.
Kellermann, M.Y., Wegener, G., Elvert, M., Yoshinaga, M.Y., Lin, Y.S., Holler, T., Mollar, X.P., Knittel, K., Hinrichs, K.U., 2012. Autotrophy as a predominant mode of carbon fixation in anaerobic methane-oxidizing microbial communities. Proc. Natl. Acad. Sci. 109, 19321–19326.
Kim, J.H., van der Meer, J., Schouten, S., Helmke, P., Willmott, V., Sangiorgi, F., Koç, N., Hopmans, E.C., Sinninghe Damsté, J.S., 2010. New indices and calibrations derived from the distribution of crenarchaeal isoprenoid tetraether lipids: implications for past sea surface temperature reconstructions. Geochim. Cosmochim. Acta 74, 4639–4654.
Kim, J.H., Villanueva, L., Zell, C., Sinninghe Damsté, J.S., 2016. Biological source and provenance of deep-water derived isoprenoid tetraether lipids along the Portuguese continental margin. Geochim. Cosmochim. Acta 172, 177–204.
Koga, Y., Morii, H., 2007. Biosynthesis of ether-type polar lipids in archaea and evolutionary considerations. Microbiol. Mol. Biol. Rev. 77, 97–120.
Kormas, K.A., Tivey, M.K., Von Damm, K., Teske, A., 2006. Bacterial and archaeal phylotypes associated with distinct mineralogical layers of a white smoker spire from a deep-sea hydrothermal vent site (9 °N, East Pacific Rise). Environ. Microbiol. 8, 909–920.
Larter, R.D., King, E.C., Leat, P.T., Reading, A.M., Smellie, J.L., Smythe, D.K., 1998. South Sandwich slices reveal much about arc structure, geodynamics and composition. EOS Trans., Am. Geophys. U. 79, 281–285.
Larter, R.D., Vanneste, L., Morris, P., Smythe, D.K., 2003. Structure and tectonic evolution of the South Sandwich arc. In: Larter, R., Leat, P.T. (Eds.), Intra-Oceanic Subduction Systems: Tectonic and Magmatic Processes. The Geological Society of London, London, pp. 255–284.
Lei, J., Chu, F., Yu, X., Li, X., Tao, C., 2016. Lipid biomarkers reveal microbial communities in hydrothermal chimney structures from the 49.6°E hydrothermal vent field at the Southwest Indian Ocean Ridge. Geomicrobiol. J. 34, 557–566.
Li, H., Lü, X., Tao, C., Han, T., Hu, P., Zhang, G., Yu, Z., Dong, C., Shao, Z., 2018. Distribution of tetraether lipids in sulfide chimneys at the Deyin hydrothermal field, southern Mid-Atlantic Ridge: implication to chimney growing stage. Sci. Rep. 8, 8060.
Li, H., Peng, X., Zhou, H., Li, J., Sun, Z., 2013. Molecular evidence for microorganisms participating in Fe, Mn, and S biogeochemical cycling in two low-temperature hydrothermal fields at the Southwest Indian Ridge. J. Geophys. Res.: Biogeosciences 118, 665–679.
Li, J., Yang, J., Sun, M., Su, L., Wang, H., Gao, J., Bal, S., 2020. Distribution and succession of microbial communities along a dispersal pathway of hydrothermal plumes on the Southwest Indian Ridge. Front. Mar. Sci. 7, 581381.
Lincoln, S.A., Bradley, A.S., Newman, S.A., Summons, R.E., 2013. Archaeal and bacterial glycerol dialkyl glycerol tetraether lipids in chimneys of the Lost City Hydrothermal Field. Org. Geochem. 60, 45–53.
Linse, K., Copley, J.T., Connelly, D.P., Larter, R.D., Pearce, D.A., Polunin, N.V.C., Rogers, A.D., Chen, C., Clarke, A., Glover, A.G., Graham, A.G.C., Huvenne, V.A., Marsh, L., Reid, W.D.K., Roterman, C.N., Sweeting, C.J., Zwirglmaier, K., Tyler, P.A., 2019. Fauna of the Kemp Caldera and its Upper Bathyal Hydrothermal Vents (South Sandwich Arc, Antarctica). R. Soc. Open Sci. 6, 191501.
Livermore, R.A., 2003. Back-arc spreading and mantle flow in the East Scotia Sea. In: Larter, R., Leat, P.T. (Eds.), Intra-Oceanic Subduction Systems: Tectonic and Magmatic Processes. The Geological Society of London, London, pp. 315–331.
Livermore, R., Cunningham, A., Vanneste, L., Larter, R., 1997. Subduction influence on magma supply at the East Scotia Ridge. Earth Planet. Sci. Lett. 150, 261–275.
Marsh, L., Copley, J.T., Huvenne, V.A., Linse, K., Reid, D.K., 2012. Microdistribution of faunal assemblages at deep-sea hydrothermal vents in the southern ocean. PLoS One 7 (10), 48348.
Marsh, L., Copley, J.T., Huvenne, V.A., Linse, K., Reid, D.K., the Isis ROV Facility, 2013. Getting the bigger picture: using precision Remotely Operated Vehicle (ROV) videography to acquire high-definition mosaic images of newly discovered hydrothermal vents in the Southern Ocean. Deep Sea Res. Part II 92, 124–135.
Marsh, L., Copley, J.T., Tyler, P.A., Thatje, S., 2015. In hot and cold water: differential life-history traits are key to success in contrasting thermal deep-sea environments. J. Anim. Ecol. 84, 898–913.
Méhay, S., Früh-Green, G.L., Lang, S.Q., Bernasconi, S.M., Brazelton, W.J., Schrenk, M. O., Schaeffer, P., Adam, P., 2013. Record of archaeal activity at the serpentinitehosted lost city hydrothermal field. Geobiology 11, 570–592.
Middleburg, J.J., 2011. Chemoautotrophy in the ocean. Geophys. Res. Lett. 38, L24604.
Naveira-Garabato, A., Heywood, K., Stevens, D., 2002. Modification and pathways of southern ocean deep waters in the Scotia Sea. Deep Sea Res. Part I 149, 681–705.
Pan, A., Qunhui, Y., Zhou, H., Ji, F., Wang, H., Pancost, R.D., 2016. A diagnostic GDGT signature for the impact of hydrothermal activity on surface deposits at the Southwest Indian Ridge. Org. Geochem. 99, 90–104.
Paraiso, J.J., Williams, A.J., Huang, Q., Wei, J., Dijkstra, P., Hungate, B.A., Dong, H., Hedlund, B.P., Zhang, C.L., 2013. The distribution and abundance of archaeal tetraether lipids in U. S. Great Basin hot springs. Front. Microbiol. 4, 247.
Pearson, A., Huang, Z., Ingalls, A., Romanek, C., Wiegel, J., Freeman, K., Smittenberg, R., Zhang, C., 2004. Non marine crenarchaeol in Nevada hot springs. Appl. Environ. Microbiol. 70, 5229–5237.
Peng, X., Chen, S., Zhou, H., Zhang, L., Wu, Z., Li, J., Li, J., Xu, H., 2011. Diversity of biogenic minerals in low-temperature Si-rich deposits from a newly discovered hydrothermal field on the ultraslow spreading Southwest Indian Ridge. J. Geophys. Res. 116, G03030.
Phleger, C.F., Nelson, M.M., Groce, A.K., Cary, S.C., Coyne, K.J., Nichols, P.D., 2005. Lipid composition of deep-sea hydrothermal vent tubeworm Riftia pachyptila, crabs Munidopsis subsquamosa and Bythograea thermydron, mussels Bathymodiolus sp. and limpets Lepetodrilus spp. Comp. Biochem. Physiol. Part B: Biochem. Mol. Biol. 141, 196–210.
Reeves, E.P., Yoshinaga, M.Y., Pjevac, P., Goldenstein, N.I., Peplies, J., Meyerdierks, A., Amann, R., Bach, W., Hinrichs, K.U., 2014. Microbial lipids reveal carbon assimilation patterns on hydrothermal sulfide chimneys. Environ. Microbiol. 16, 3515–3532.
Rogers, A.D., Tyler, P.A., Connelly, D.P., Copley, J.T., James, R., Larter, R.D., Linse, K., Mills, R.A., Naveira Garabato, A., Pancost, R.D., Pearce, D.A., Polunin, N.V.C., German, C.R., Shank, T., Boersch-Supan, P.H., Alker, B.J., Aquilina, A., Bennet, S.A., Clarke, A., Dinley, R.J.J., Graham, A.G.C., Green, D.R.H., Hawkes, J.A., Hepburn, L., Hilario, A., Huvenne, V.A.I., Marsh, L., Ramirez-Llodra, E., Reid, W.D.K., Roterman, C.N., Sweeting, C.J., Thatje, S., Zwirglmaier, K., 2012. The discovery of new deep-sea hydrothermal vent communities in the Southern Ocean and implications for biogeography. PLoS Biol. 10, e1001234.
Schouten, S., Baas, M., Hopmans, E.C., Sinninghe Damsté, J.S., 2008. An unusual isoprenoid tetraether lipid in marine and lacustrine sediments. Org. Geochem. 39, 1033–1038.
Schouten, S., Hopmans, E.C., Pancost, R.D., Sinninghe Damsté, J.S., 2000. Widespread occurrence of structurally diverse tetraether membrane lipids: evidence for the ubiquitous presence of low-temperature relatives of hyperthermophyles. Proc. Natl. Acad. Sci. 97, 14421–14426.
Schouten, S., Hopmans, E.C., Schefuβ, E., Sinninghe Damsté, J.S., 2002. Distributional variations in marine crenarchaeotal membrane lipids: a new organic proxy for reconstructing ancient sea water temperatures? Earth Planet. Sci. Lett. 204, 265–274.
Schouten, S., Hopmans, E.C., Sinninghe Damsté, J.S., 2013. The organic geochemistry of glycerol dialkyl glycerol tetraether lipids: a review. Org. Geochem. 54, 19–61.
Schouten, S., Pitcher, A., Hopmans, E.C., Villanueva, L., van Bleijswijk, J., Sinninghe Damsté, J.S., 2012. Intact polar and core glycerol dibiphitanyl glycerol tetraether lipids in the Arabian Sea oxygen minimum zone: I. Selective preservation and degradation in the water column and consequences for the TEX_{86}. Geochim. Cosmochim. Acta 98, 228–243.
Schouten, S., van der Meer, M.T., Hopmans, E.C., Rijpstra, W.I., Reysenbach, A.L., Ward, D.M., Sinninghe Damsté, J.S., 2007. Archaeal and bacterial glycerol dialkyl glycerol tetraether lipids in hot springs of Yellowstone national park. Appl. Environ. Microbiol. 73, 6181–6191.
Schouten, S., Wakeham, S.G., Hopmans, E.C., Sinninghe Damsté, J.S., 2003. Biogeochemical evidence that thermophilic archaea mediate the anaerobic oxidation of methane. Appl. Environ. Microbiol. 69, 1680–1686.
Schrenk, M.O., Kelley, D.S., Delaney, J.R., Baroos, J.A., 2003. Incidence and diversity of microorganisms within the walls of an active deep-sea sulfide chimney. Appl. Environ. Microbiol. 69 (6), 3580–3592.
Siliakus, M.F., van deer Oost, J., Kengen, S.W.M., 2017. Adaptations of archaeal and bacterial membranes to variations in temperature, pH and pressure. Extremophiles 21, 651–670..
Simoneit, B.R.T., Lein, A.Y., Peresypkin, V.I., Osipov, G.A., 2004. Composition and origin of hydrothermal petroleum and associated lipids in the sulphide deposits of the

Rainbow Field (Mid-Atlantic Ridge at 36 oN). Geochim. Cosmochim. Acta 68, 2275–2294.
Sinninghe Damsté, J.S., Rampen, S., Irene, W., Rijpstra, C., Abbas, B., Muyzer, G., Schouten, S., 2003. A diatomaceous origin for long-chain diols and mid-chain hydroxy methyl alkanoates widely occurring in quaternary marinesediments: indicators for high-nutrient conditions. Geochim. Cosmochim. Acta 67 (7), 1339–1340.
Sollich, M., Yoshinaga, M.Y., Häusler, S., Price, R.E., Hinrich, K.U., Büring, S.I., 2017. Heat stress dictates microbial lipid composition along a thermal gradient in marine sediments. Front. Microbiol. 8, 1550.
Thomas, C., Livermore, R., Pollitz, F., 2003. Motion of the Scotia Sea plates. Geophys. J. Int. 155, 789–804.
Tierney, J.E., Tingley, M.P., 2015. A TEX_{86} surface sediment database and extended Bayesian calibration. Sci. Data 29, 150029..
Turich, C., Freeman, K.H., Bruns, M.A., Conte, M., Jones, A.D., Wakeham, S.G., 2007. Lipids of marine Archaea: patterns and provenance in the water-column and sediments. Geochim. Cosmochim. Acta 71, 3272–3291.
Uda, I., Sugai, A., Itoh, Y.H., Itoh, T., 2004. Variation in molecular species of core lipids from the order *Thermoplasmales* strains depends on the growth temperature. J. Oleo Sci. 53, 399–404.
Umoh, U.U., Li, L., Luckge, A., Schwartz-Schampera, U., Naafs, B.D.A., 2020. Influence of hydrothermal vent activity on GDGT pool in marine sediments may be less than previously thought. Org. Geochem. 149, 104102.
Villanueva, L., Sinninghe Damsté, J.S., Schouten, S., 2014. A re-evaluation of the archaeal membrane lipid biosynthetic pathway. Nat. Rev. Microbiol. 12, 438–448.
Watanabe, H.K., Shigeno, S., Fujikura, K., Matsui, T., Kato, S., Yamamoto, H., 2019. Faunal composition of deep-sea hydrothermal vent fields on the Izu–Bonin–Mariana Arc, northwestern Pacific. Deep Sea Res. Part I 149, 1–6.
Wu, W., Zhang, C.L., Wang, H., He, L., Li, W., Dong, H., 2013. Impacts of temperature and pH on the distribution of archaeal lipids in Yunnan hot springs, China. Front. Microbiol. 4, 312.
Zeng, Z., Liu, X.-L., Farley, K.R., Wei, J.H., Metcalf, W.W., Summons, R.E., Welander, P. V., 2019. GDGT Cyclization Proteins Identify the Dominant Archaeal Sources of Tetraether Lipids in the Ocean. Proc. Natl. Acad. Sci. 116 (45), 22505–22522.
Zwirglmaier, K., Reid, W.D.K., Heywood, J., Sweeting, C.J., Wigham, B.D., Polunin, N.V. C., Hawkes, J.A., Connelly, D.P., Pearce, D., Linse, K., 2015. Linking regional variation of epibiotic bacterial diversity and trophic ecology in a new species of Kiwaidae (Decapoda, Anomura) from East Scotia Ridge (Antarctica) hydrothermal vents. Microbiol. Open 4, 136–150.